Nano Progress

Ariviyal Publishing

Research Article

DOI: 10.36686/Ariviyal.NP.2020.02.04.020

Nano Prog., (2020) 2(4), 58-63.

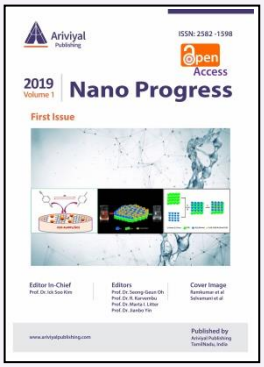

Evaluation of Structural and Electrical Properties of Ball-milled $NaNbO_3$ Ceramic

Sumit K. Roy[a] and Kamal Prasad*[b]

[a]*Department of Physics, St. Xavier's College, Ranchi, 834001, India*

[b]*University Department of Physics, T.M. Bhagalpur University, Bhagalpur, 812007, India*

***Corresponding author E-mail address**: prasad_k@tmbuniv.ac.in (K. Prasad)

ISSN: 2582-1598

Crossref

Publication details
Received: 25th October 2020
Revised: 1st December 2020
Accepted: 1st December 2020
Published: 11th December 2020

Abstract: This work reports the effect of milling on the structural, microstructural, electrical, and piezoelectric properties of $NaNbO_3$ (NN) ceramics synthesized using a solid-state reaction method. X-ray diffraction studies exhibited that the lattice structure of milled and un-milled NN samples is orthorhombic with a space group *Pmc*21. The average particle size and lattice strain were found to 203 nm and 0.05 un-milled samples whereas they were 37 nm and 0.2 for 10 h milled samples. FTIR spectra indicated a shift in peak position with milling time. SEM image showed the formation of small grains ~1.2 µm for 10 h milled NN samples which is advantageous for dielectric applications in high density integrated circuits. An increase in the values of dielectric constant from 377 to 698, d_{33} from 29 to 37, and a drop in critical temperature from 426°C to 352°C at 1 kHz were registered for un-milled and milled samples. A negative temperature coefficient of resistance behaviour was noticed from the impedance and ac conductivity analyses. The correlated barrier hopping model successfully explains the charge transport mechanism in the present ceramic system and ac conductivity data obeyed Jonscher's universal power law. A marked increment in d_{33} with smaller particle size was observed with the increasing milling hour that could make NN a promising lead-free piezoelectric material for piezo-sensing/detection and energy harvesting applications.

Keywords: $NaNbO_3$; lead-free electroceramic; milling; structure; dielectric; piezoelectric

1. Introduction

Among the techniques used to synthesize nanomaterials today, mechanical-chemical, chemical, flame combustion, hydrothermal, emulsion precipitation, and solvothermal are seen as the most widely used processes where each method varies in their effectiveness. While synthesizing different nanoparticles, there has always been a confrontation between the achievement of a compound in the purest form/phase and the minimization of particle size. Among these, mechanical alloying is considered as the industrially viable method of nanomaterial synthesis. Likewise, among mechanical alloying and high-temperature solid-state reaction (SSR) technique, the purity of phase and minimization of size seems to be conjugate pairs and simultaneously non-doable. In SSR method where a pure phase could be obtained but the particles usually remain larger (~µm) and inhomogeneous, whereas, in mechanical alloying where long hours of milling reduce the particle size to nanoscale, it is hard to achieve a pure phase due to contamination via the walls of the jar, the balls used for size reduction and few unreacted species. Here, we have opted for a modality where a perfect balance could be maintained between the purity of the phase and minimization of the size, an approach where particle size can be cut to a minimum without compromising with the purity of form. There has been a strong demand, especially from the last few decades, to develop lead-free compounds for piezoelectric applications for environmental reasons.[1-3]

Sodium niobate ($NaNbO_3$; abbreviated hereafter as NN), an alkaline niobate ceramic is considered to be a potent and might be considered as a technologically important alternative to commercial Pb-containing piezoelectric ceramics, as it exhibits phase transitions between paraelectric, antiferroelectric and ferroelectric phases.[4,5] Castro *et al.*[6] synthesized NN nanoparticles mechanically in a vibrating-type mill while Hungria *et al.*[7] stoichiometrically mixed Nb_2O_5 and different reactants of sodium (Na_2CO_3, Na_2O, and NaOH) by mechanically activated high-energy milling to obtain powders of NN ceramic. Also, Rojac *et al.*[8] synthesized 10–20 nm sized NN ceramic powders mechanochemically using the constituents (Na_2CO_3 and Nb_2O_5) in a planetary mill for 40 h. Besides, Yun *et al.*[9] prepared NN powder by mechanical alloying from commercially available Na_2CO_3 and Nb_2O_5 powders by using WC balls. They eventually reduced the time required to synthesize NN to below 120 mins and synthesized 10–20 nm powder. A substantial number of research groups also engaged themselves in synthesizing NN by the SSR method. Hsiao *et al.*[10] obtained pure NN by direct pressing and sintering raw materials at 1100-1200°C. Also, Koruza *et al.*[11] prepared NN by SSR method and exclusively examined the structural

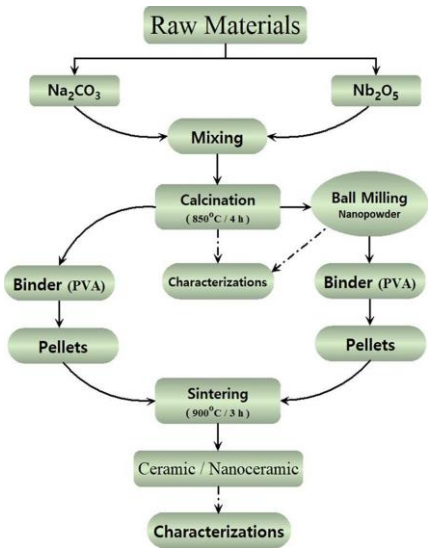

Fig. 1. Schematics for the synthesis of $NaNbO_3$ ceramic and nanoceramic using high energy ball milling method.

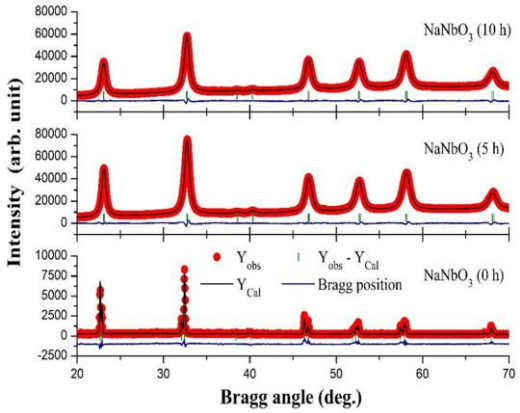

Fig. 2. Room temperature X-ray diffraction patterns of $NaNbO_3$ ceramic powders at different milling times.

behaviour below 400°C and detected four-phase transitions, taking place mainly due to the movement of Na that occupy the more symmetric position as well as a little change in the tilting system. Further, a marginally different path was taken up by Chaiyo *et al*.[12] where they prepared NN powders by an improvised SSR method where the $Na_2C_2O_4$ and Nb_2O_5 mixture were heated at 475°C/1 h and obtained mean crystallite size of 31.45±5.28 nm. A lowering of temperature by about 300°C was observed compared to the conventional SSR method. Recently, the synthesis of single-phase orthorhombic perovskite NN ceramic with the space group *Pmmm* has been reported by Roy *et al*.[13] In another study, Koruza *et al*.[14] prepared NN nanopowder (size ~25 nm) by simple optimized top-down processing by the amalgamation of the SSR synthesis followed by milling. Yang *et al*. [15], in a very recent work, discussed the dielectric energy storage applications of lead-free antiferroelectric ceramic, $NaNbO_3$. Also, Gyan *et al*.[16] achieved stabilization of the antiferroelectric phase in $NaNbO_3$ against the set pattern prescribed by researchers earlier.

With the aim to see the effect of milling on the structure, microstructure, electric and piezoelectric properties single-phase ceramic powder of NN was prepared using an SSR route. It was then milled up to the optimum level and the as-milled NN ceramic was characterized using X-ray diffraction, scanning electron microscope, infrared spectroscopy, dielectric, impedance, ac conductivity, and piezoelectric studies.

2. Experimental Section

2.1. Preparation of $NaNbO_3$ ceramic powders

The ceramic powders of NN were prepared using a standard SSR method and the corresponding nanoceramic powders were obtained through the ball milling technique. Fig. 1 details the process adopted for the fabrication of NN ceramic and nanoceramic as well as their powders. To this end, reagent grade (>99.9 % purity) Na_2CO_3 and Nb_2O_5 were used as starting materials. These ingredients were first thoroughly mixed in the dry condition in an agate mortar and pestle and then in a planetary mill in a methanol medium for 15 minutes. The obtained slurry was dried and then calcined at 850°C for 5 h in air atmosphere. The completion of the reaction and the formation of the desired compound were ascertained by an X-ray diffraction (XRD) technique. The as-calcined powder was then subjected to high energy milling in a Retsch, Germany make planetary ball mill using a tungsten carbide (WC) vial and WC balls of 10 mm diameter, keeping the ball to - powder weight ratio to be 30:1 with 300 rpm milling speed giving an interval break of 5 min. followed by reverse rotation in each hour. The milled powders were taken out at different milling times, *i.e*. 0, 5, and 10 h, for their XRD and infrared (IR) spectroscopic analysis and are denoted, hereafter as NN-0, NN-5, and NN-10, respectively. Further, a small amount of polyvinyl alcohol was added as a binder to the un-milled and milled powders and then compacted into thin (~1.25 mm) circular disks with an applied uniaxial pressure of 650 MPa. Thereafter, the compacted pellets of NN-0 and NN-10 were sintered, respectively at 870°C/3h and 820°C/2.5h in the air atmosphere.

2.2. Characterization of $NaNbO_3$ Nanoceramic

The XRD data of NN-0, NN-5, and NN-10 powders were obtained by X-ray diffractometer (XPERT-PRO, Pan Analytical, USA) at room temperature, using CuKα radiation (λ = 1.5405 Å) over a wide range of Bragg angles (20° ≤ 2θ ≤ 70°). The Fourier transformed infrared (FTIR) spectra of all the specimens were obtained in the range of 500–5000 cm^{-1} by an Alpha-T Bruker FTIR spectrophotometer in the transmission mode. A JEOL-JSM840A, Japan make scanning electron microscope (SEM) was used to acquire the SEM micrographs of the fractured surfaces of NN-0 and NN-10 ceramics. Further, the symmetrical Ag|NN-0/NN-10|Ag cells, where Ag is a conductive paste (Ted Pele, USA) coated on either side of the polished sintered pellets, were prepared for the impedance measurements. The frequency (20 Hz – 10 MHz) and temperature (20°C – 500°C) dependent impedance measurements were carried out using a computer-interfaced impedance analyzer (E4990A-120, Keysight Technologies, USA). The ac conductivity data were obtained using the relation $\sigma_{ac} = 2\pi f \varepsilon_o \varepsilon''$, here f is the operating frequency, ε_o = 8.85×10^{-12} F/m is the dielectric constant of the free space, ε' and ε''

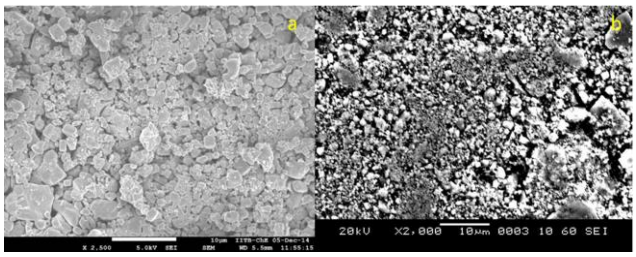

Fig. 3. SEM images of un-milled (0 hr) and milled (10 hr) $NaNbO_3$ ceramic powder.

are, respectively the real and imaginary parts of dielectric constant and tanδ (= $\varepsilon''/\varepsilon'$) is the dielectric tangent loss. The samples were poled in silicone oil at 25°C under an electric field of 2.5 kV/mm for 15 min. The longitudinal piezoelectric charge coefficient (d_{33}) was measured using a d_{33} meter (PM3500; KCF Technologies, USA).

3. Results and Discussions

3.1. Structure and microstructure studies

Rietveld refined XRD profiles of NN-0, NN-5, and NN-10 are presented in Fig. 2. The Rietveld refinement of XRD data of NN-0 suggested that it is a pure perovskite phase with an orthorhombic structure (space group *Pmc*21) with the lattice parameters a = 7.79 Å, b = 5.51 Å, and c = 5.56 Å. Also, a significant peak broadening without any change in the lattice parameters is observed with the increase in milling hours. The broadening of XRD profiles with longer milling times is evidence of decrement of particle size and the development of lattice strain in the material. The values of apparent particle sizes and lattice strains were estimated using Williamson-Hall equation: $B\cos\theta = (K\lambda/D) + 2(\Delta\xi/\xi)\sin\theta$; here B is the diffraction peak width at half intensity, $\Delta\xi/\xi$ is the lattice strain, K (= 0.89) is the Scherrer constant and the term $K\lambda/D$ represents the Scherrer particle size distribution. The average particle size of the NN-0 was estimated to be ~203 nm, whereas it is 42 nm and 37 nm, respectively, for NN-5 and NN-10. Also, the lattice strain was found to increase from 0.05 (for NN-0) to 0.2 (for NN-10).

SEM images of NN-0 and NN-10 ceramics shown in Fig. 3 provide considerable information regarding the texture, grains, and density of the materials. The average grain size, measured using a linear intercept method, is found to be in the range of 0.8 to 2.5 μm and 0.5 to 1.4 μm, relatively for NN-0 and NN-10. The reduction in grain sizes for NN-10 maybe because some stress might have produced during high energy milling. This generated stress could prevent grain boundary movement during the sintering and thereby result in the reduction of grain size.

The infrared spectra of NN-0, NN-5, and NN-10 samples are depicted in Fig. 4. It is noticed that with the increase in milling hour the fraction of fine particles increases, the ceramic becomes dense, absorbance increases and in turn, transmittance decreases. All the prominent peaks are found to follow this trend. The peak at 633 cm^{-1} in NN-0 corresponds to the metal oxide *i.e.* Nb-O bond.[12,17] A shift in the peak position is observed with milling time and the wavenumber corresponding to the Nb-O bond for NN-10 is 573 cm^{-1}. The shift in wavenumber may be due to the difference in natural frequencies of

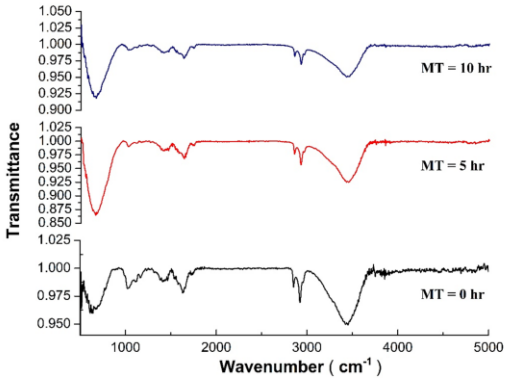

Fig. 4. Room temperature FTIR spectra of $NaNbO_3$ ceramic powders at different milling times.

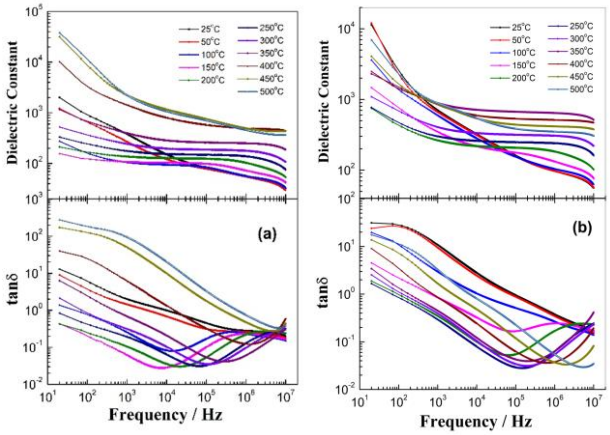

Fig. 5. Frequency dependence of dielectric constant and loss tangent of (a) un-milled and (b) 10 h milled $NaNbO_3$ ceramic samples at different temperatures.

atoms in micro and nanoceramics as natural frequency depends on a number of factors like dipole interactions, interfacial effects, and surface free energy.[18] With milling time as grain size decreases and surface to volume ratio increases, the atomic arrangement on the surface differs from the bulk crystal.

3.2. Dielectric and piezoelectric studies

The frequency response of ε' and tanδ of NN-0 and NN-10 at different temperatures are depicted in Figs. 5a and 5b. From the plots, it can be inferred that ε' varies inversely with frequency for both the ceramics. At high frequencies comparatively low value of ε' is a common behavior of dielectric/ferroelectric materials as it is not possible for the dipoles within the samples to respond in consonance with the operating frequencies $\gtrsim$ MHz. The overall dipole moment and thus electric polarization decreases which in turn lowers the values of dielectric constant. The variation tanδ in the low and high-frequency region is seen to be different. At lower frequencies, tanδ decreases with an increase in frequency and then increases with an increase in frequency and ultimately it attains a maximum at MHz region. Also, the peak position (ε''_{max}) shifts towards the higher frequency side with the increase in temperature indicating the increasing loss in the sample. Such a variation could be explained on the fact that there is a distinct effect of frequency and temperature

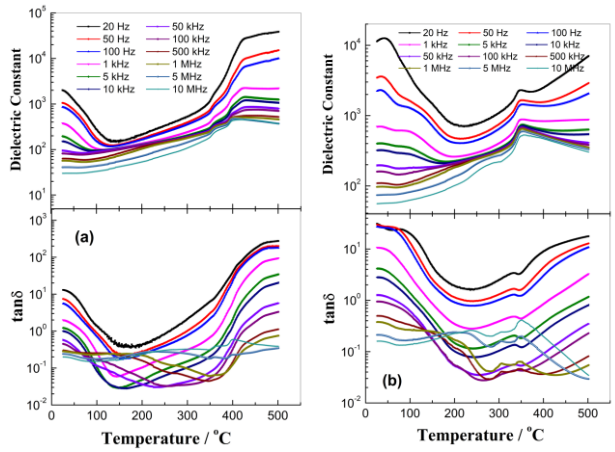

Fig. 6. Temperature dependence of dielectric constant and loss tangent of (a) un-milled and (b) 10 h milled $NaNbO_3$ ceramic samples at different frequencies.

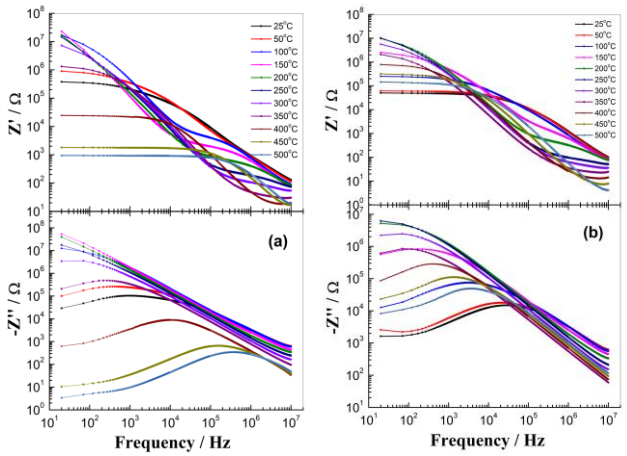

Fig. 7. Frequency dependence of real and imaginary parts of impedance of (a) un-milled and (b) 10 h milled $NaNbO_3$ ceramic samples at different temperatures.

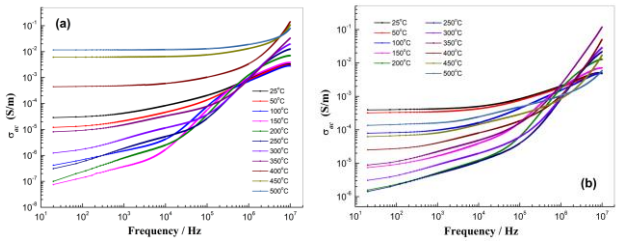

Fig. 8. Frequency dependence of ac conductivity of (a) un-milled and (b) 10 h milled $NaNbO_3$ ceramic samples at different temperatures.

on the electrical conductivity and dielectric relaxations in a material which are given as $\varepsilon'' = \sigma/\omega\varepsilon_o = (\sigma_d + \sigma_i)/\omega\varepsilon_o$, and consequently, the expression $\varepsilon^* = \varepsilon' - i\varepsilon''$ could be written as:[19] $\varepsilon^* = \varepsilon' - i(\varepsilon'' + \sigma_i/\omega\varepsilon_o)$; here σ_d and σ_i represent conductivity due to dipole relaxation and ionic drift, respectively.

The variation of ε' and tanδ with the temperature at different frequencies are shown in Figs. 6a and 6b for NN-0 and NN-10, respectively. It is seen that the ferroelectric-to-paraelectric phase transition temperature (T_m) decreases in all the frequency values with the increase in milling time. The value of T_m at 1 kHz, dropped from 426°C for NN-0 to 352°C for NN-10. A low value of T_m simply implies that less energy is required for a phase transition in the milled sample. The mechanical energy received by the sample during the milling is stored in it in the form of surface and/or grain boundary energy as the milled sample contains smaller grains. The dispersion in ε'-T graph is minimum near the T_m and increases in either side as we move away from it for both the samples and is observed to be more prominent in the milled sample. Also, it is seen that the T_m shifts towards the lower values with the decrease in frequency which indicates that less amount of energy is required for phase transition at a lower frequency. Besides, the value of ε' at room temperature for NN-10 (698) is found to be greater than that of NN-0 (377). This may be due to the fact that the grain sizes decrease with milling that allows grain boundary contribution to increase.[20,21] Further, the grain boundary which serves as structural discontinuity weakens the coupling between adjacent local permanent electric dipoles within the grains in the samples, which makes it easier for the electric dipoles to align themselves along the field when an external alternating electric field is applied, enhancing the dielectric responses. The d_{33} values of poled NN-0 were found to increase from 29 pC·N^{-1} to 37 pC·N^{-1} for poled NN-10.

3.3. Electric impedance studies

Figs. 7a and 7b show the variation of the real (Z') and imaginary (Z'') parts of impedance with frequency at different temperatures, respectively for NN-0 and NN-10. The values of Z' were observed to decrease with the increase in frequency for all the temperatures, which indicates an increase in the σ_{ac} with the rise in frequency. Also, in the low-frequency region and at higher temperatures, Z' values are approximately constant. Further, the value of Z' decreases with the rise of temperature clearly displays the negative temperature coefficient of resistance (NTCR) character for both NN-0 and NN-10. Further, the values of Z'' monotonically decrease with frequency at lower temperatures, and at and above 150ºC the values of Z'' reach a maximum peak (Z''_{max}) which shifts towards the high-frequency side with the increase in temperature in both the samples. Also, it is noticed that the frequency corresponding to Z''_{max} has a lower value for NN-10 compared to NN-0 corresponding to each temperature value. Hence, relaxation takes place at a lower frequency in the milled sample.

3.4. Ac conductivity studies

Figs. 8a and 8b, respectively illustrate the frequency dependence of the σ_{ac} of NN-0 and NN-10 at different temperatures in the logarithmic scale. It is well-known that the ac conductivity in most of the materials due to localized states, comprises of the dc-component (σ_o; frequency-independent) in the low-frequency region and the frequency-dependent ac-component ($A\omega^s$; s is an index) following Jonscher's power law: $\sigma_{ac} = \sigma_o + A\omega^s$. A shift from the frequency-independent to frequency-dependent regions could be observed in both the cases exhibiting the onset of the conductivity relaxation

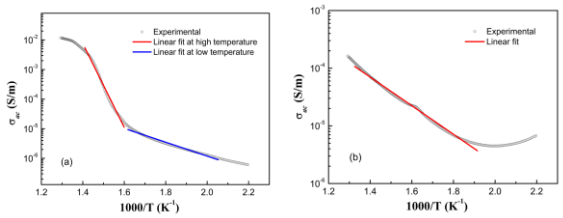

Fig. 9. Temperature dependence of ac conductivity of $NaNbO_3$ ceramics at 1kHz prepared with (a) un-milled and (b) 10 h milled powders.

phenomenon, indicating the transition from long-range hopping to the short-range ion-motion. Also, the values of σ_{ac} increase with increasing frequency at each temperature that may be due to the increased mobility of oxygen vacancies or other structural defects. The values of σ_o were found to be ~1.38 x 10^{-5} S/m for NN-0 and ~3.3 x 10^{-4} S/m for NN-10 at 50°C. Hence, the milled sample has a lower dc resistivity value than an un-milled sample at each temperature. The milled sample offers a low dc resistivity as the charge carriers in it are at higher energy state and it is easier for them to hop.

Further, the mechanism of hopping conduction is generally consistent with the presence of a high density of states in the materials having band-gap like that of semiconductors where the formation of polarons takes place and the hopping conduction may occur between the nearest neighbouring sites due to localization of charge carriers. Figs. 9a and 9b, respectively depict the variation of σ_{ac} versus $10^3/T$ for NN-0 and NN-10 at 1 kHz. It is seen that the magnitude of σ_{ac} increases with the rise of temperature, which clearly indicated the NTCR character of the samples. The activation energy for conduction was obtained using the Arrhenius relationship: $\sigma_{ac} = \sigma_o \exp(-E_a / k_B T)$. Linear least-squares fitting of the ac conductivity data to the above equation gave the value of the apparent activation energy E_a. The values of E_a, as estimated from the Arrhenius plots for NN-0 at high temperature is 1.22 eV and at low temperature, it is 0.47 eV while NN-10 exhibits moderately constant activation energy over the entire temperature range and is found to be 0.15 eV. The low value of E_a in the milled sample is due to the carrier transport through hopping between localized states in a disordered manner.

4. Conclusions

Polycrystalline $NaNbO_3$ (NN) ceramics, prepared by a high-temperature solid-state reaction route and high energy milling with different milling hours, were found to possess a perovskite-type orthorhombic structure. FTIR spectra confirmed the formation of NN. An increase in the values of dielectric constant from 377 to 698, d_{33} from 29 to 37, and a drop in the critical temperature from 426°C to 352°C at 1 kHz were noticed for un-milled and milled samples. A negative temperature coefficient of resistance behaviour was observed from the impedance and ac conductivity analyses. The correlated barrier hopping model successfully explains the charge transport mechanism in the present ceramic system, and ac conductivity data obeyed Jonscher's universal power law. A marked increment in d_{33} with smaller particle size was observed, with the increase of the milling time and, therefore, NN-10 offers a promising alternative lead-free piezoelectric material for piezo-sensing/detection and energy harvesting applications. Besides, the optimization of the milling conditions where the minimum particle size can be achieved without any contamination is only the major concern in such a process. In summary, proper high energy milling of such electroceramic led to having multifold advantages such as improvement in the homogeneity, reduction in the particle as well as grain sizes, and superior electric and piezoelectric properties.

Conflicts of Interest

The authors declare that they have no conflict of interest.

References

1 Saito Y.; Takao H.; Tani T.; Nonoyama T.; Takatori K.; Homma T.; Nakamura M. High Performance Lead-Free Piezoelectric Material. *Nature*, 2004, **432**, 84-87. [Link]
2 Ringgaard E.; Wurlitzer T. Lead-Free Piezoceramics Based on Alkali Niobates. *J. Euro. Ceram. Soc.*, 2005, **25**, 2701-2706. [CrossRef]
3 Mahto U.K.; Roy S.K.; Prasad K. High Energy Milled $Ba_{0.06}Na_{0.47}Bi_{0.47}TiO_3$ Ceramic: Structural and Electrical Properties. *IEEE Trans. Dielectr. Electr. Insul.*, 2018, **25**, 174-180. [CrossRef]
4 Dungan R.H.; Golding R.D. Metastable Ferroelectric Sodium Niobate. *J. Am. Ceram. Soc.*, 1964, **47**, 73-76. [CrossRef]
5 Glazer A.M.; Megaw H.D. Studies of the Lattice Parameters and Domains in the Phase Transitions of $NaNbO_3$. *Acta Cryst. Sec. A: Cryst.*, 1973, **29**, 489-495. [CrossRef]
6 Castro A.; Jimenez B.; Hungrıa T.; Moure A.; Pardo L. Sodium Niobate Ceramics Prepared by Mechanical Activation Assisted Methods. *J. Eur. Ceram. Soc.*, 2004, **24**, 941-945. [CrossRef]
7 Hungría T.; Pardo L.; Moure A.; Castro A. Effect of Mechanochemical Activation on the Synthesis of $NaNbO_3$ and Processing of Environmentally Friendly Piezoceramics. *J. Alloys Compd.*, 2005, **395**, 166-173. [CrossRef]
8 Rojac T.; Kosec M.; Malič B.; Holc J. Mechanochemical Synthesis of $NaNbO_3$. *Mater. Res. Bull.*, 2005, **40**, 341-345. [CrossRef]
9 Yun J.Y.; Jeon J.H.; Kang S.J.L. Synthesis of Sodium Niobate Powders by Mechanochemical Processing. *Mater. Trans.*, 2008, **49**, 2166-2168. [CrossRef]
10 Hsiao Y.J.; Chang Y.H.; Chang Y.S.; Fang T.H.; Chai Y.L.; Chen G.J.; Huang T.W. Growth and Characterization of $NaNbO_3$ Synthesized using Reaction-Sintering Method. *Mater. Sci. Eng.: B*, 2007, **136**, 129-133. [CrossRef]
11 Koruza J.; Tellier J.; Malič B.; Bobnar V.; Kosec M. Phase Transitions of Sodium Niobate Powder and Ceramics, Prepared by Solid State Synthesis. *J. Appl. Phys.*, 2010, **108**, 113509-9. [CrossRef]
12 Chaiyo N.; Boonchom B.; Vittayakorn N. Solid-State Reaction Synthesis of Sodium Niobate ($NaNbO_3$) Powder at Low Temperature. *J. Mater. Sci.*, 2010, **45**, 1443-1447. [CrossRef]
13 Roy S.K.; Singh S.N.; Kumar K.; Prasad K. Structural, FTIR and Ac Conductivity Studies of $NaMeO_3$ (Me ≡ Nb, Ta) Ceramics. *Adv. Mater. Res.*, 2013, **2**, 173-180. [CrossRef]
14 Koruza J.; Malič B.; Noshchenko O.; Kosec M. Top-Down Processing of $NaNbO_3$ Nanopowder. *J. Nanomater.*, 2012, **2012**, 3, 7 pages. [CrossRef]
15 Yang D.; Gao J.; Shu L.; Liu Y.; Yu J.; Zhang Y.; Li J. F. Lead-Free Antiferroelectric Niobates $AgNbO_3$ and $NaNbO_3$ for Energy Storage Applications. *J. Mater. Chem.* A, 2020, **8**, 23724-23737. [CrossRef]
16 Gyan D.S.; Sharma P.; Dwivedi A. Effect of Octahedral Tilting on Antiferroelectric Phase Stabilization in (1-*x*)$NaNbO_3$-*x*$CdTiO_3$ Ceramics. *J. Phys. D: Appl. Phys.*, 2020, **53**, 335305. [CrossRef]
17 Vlazan P.; Sfirloaga P.; Rus F.S. Synthesis and Characterization of Lead-Free Sodium Niobate Powder. *Studia UBB Chemia*, 2016, **61**, 33-41. [Link]
18 Kumar P.; Murty B.S.; Rajan K.M. Infrared and Structural Studies of Micro and Nano-Crystalline Ta Doped Lead Zirconate Titanate Ceramics. *Defence Sci. J.*, 2018, **68**, 412-416. [Link]

19 Gabriel C.; Gabriel S.; Grant E.H.; Halstead B.S.J.; Mingos D.M.P. Dielectric Parameters Relevant to Microwave Dielectric Heating. *Chem. Soc. Rev*., 1998, **27**, 213-223. [CrossRef]
20 Mahto U.K.; Roy S.K.; AmarNath K.; Prasad K. Effect of High-Energy Ball Milling on the Electrical Properties of $NaTaO_3$ Ceramic. *Process. Appl. Ceram*., 2016, **10**, 143-152. [CrossRef]
21 Uchino K.; Sadanaga E.; Hirose T. Dependence of the Crystal Structure on Particle Size in Barium Titanate. *J. Am. Ceram. Soc*., 1989, **72**, 1555-1558. [CrossRef]